JOURNAL OF CATALYSIS 87, 363–380 (1984)

Surface Intermediates in Selective Propylene Oxidation and Ammoxidation over Heterogeneous Molybdate and Antimonate Catalysts

J. D. BURRINGTON, C. T. KARTISEK, AND R. K. GRASSELLI

Research Department, The Standard Oil Company (Ohio), 4440 Warrensville Center Road, Cleveland, Ohio 44128

Received August 12, 1983

The influence of the ammonia/propylene feed ratio on the acrylonitrile/acrolein product ratio for bismuth molybdate-based catalysts indicates the presence of two mechanistic regimes. One of these occurs under normal, high turnover conditions and corresponds to a catalytic site composed of one Mo-diooxo group (the O-inserting species) which activates ammonia by formation of a Mo-diimido which is the active N-inserting species. The other regime at lower turnovers (by He or N_2 dilution of feed) utilizes two Mo-dioxo or -diimido species at the active site, in which one Mo species acts as an O- or N-inserting element, and the other serves as a redox element to facilitate catalyst reduction and reoxidation. In both regimes, bridging Bi^{3+}–O species serve as the α-H-abstracting element to form initially a Mo–π-allyl in the rate-determining step. Similar experiments on antimonate catalysts reveal that, over the entire range of experimental conditions, active sites are composed of bridging O- (or N-) inserting atoms associated with two Sb^{5+} atoms, which are bonded by a H-abstracting Sb^{3+}–O bridge. Ammonia activation occurs by successive formation of two bridging NH groups, the N-inserting species. The isotope effects for the second H abstraction for ammoxidation over molybdate ($k_H/k_D = 2.1$) and antimonate ($k_H/k_D = 1.4$) systems indicate that reversible N insertion of allyl into an unsaturated Mo=NH species occurs (i.e., $\pi \rightleftarrows \sigma$), but a more irreversible insertion into a bridging Sb–NH–Sb species (i.e., $\pi \rightarrow \sigma$) is favored. The isotopic distribution (d_2/d_0) of acrylonitrile produced from allylic-deuterated propylene, allyl alcohol, and allylamine reveals that allylic scrambling for propylene and allyl alcohol, but C–N bond retention for allyl amine, occur due to favored allyl migration from O to N, but H migration from N to O, in the molybdate surface intermediates.

INTRODUCTION

The selective oxidation and ammoxidation of olefins have been the subject of much commercial interest and mechanistic study for the past 20 years (*1*). The selective ammoxidation of propylene to acrylonitrile,

$$CH_3CH{=}CH_2 + NH_3 + \tfrac{3}{2}O_2 \xrightarrow[\text{catalyst}]{400\text{–}460^\circ C} CH_2{=}CHCN + 3H_2O \quad (1)$$

produced at a rate of 8 billion lbs./year, is the most commercially significant reaction of this type. The mechanistically related oxidation reaction

$$CH_3CH{=}CH_2 + O_2 \xrightarrow[\text{catalyst}]{300\text{–}450^\circ C} CH_2{=}CHCHO + H_2O \quad (2)$$

produces acrolein, also an important chemical intermediate. Generally, the same catalysts can be used for either reaction. The most active and selective catalyst systems for these reactions are based on oxides of either molybdenum (e.g., $Bi_2Mo_3O_{12}$) or antimony (Fe–Sb–O_x). While both the molybdate and antimonate systems have received much mechanistic attention and analogies of the two types of catalysts have been discussed (*2*), a critical comparison of the key features of each in terms of the nature of the active sites, the selective surface intermediates, and the modes of decomposition to selective products is not available in current literature. It is the object of this work to make such a comparison based on critical differences between the ammoxidation

0021-9517/84 $3.00

and oxidation reaction for both Mo- and Sb-based systems as a probe for active site structures and bonding, NH_3 activation, and O- and N-insertion steps.

Previous mechanistic work for molybdate systems (Scheme 1) reveals that the active sites for selective oxidation (**1**) are composed of Mo-dioxo groups, which are the propylene-chemisorption and the O-insertion sites, bridged to Bi–O groups, which are the sites for rate-determining α-H abstraction (*1*). This allylic H abstraction results in the initial formation of a π-allylic molybdate intermediate (**2**) which is in rapid equilibrium with the σ-O form (**3**), the acrolein precursor. Allyl alcohol has been used to probe the σ-O allyl species (**3**) (*3*) in this mechanistic scheme. In ammoxidation, ammonia is activated by formation of an imido (Mo=NH) species (**4**). The reaction to form acrylonitrile then proceeds via the analogous N-π (**5**) and σ-allyl (**6**) species.

The dependence of the acrolein/acrylonitrile ratio on the ammonia/propylene feed ratio is kinetically related to the number of ammonia molecules activated per site in the acrylonitrile-forming cycle (*4*). A detailed analysis of this effect has been performed as a probe for the nature and number of atomic components at the active sites for ammonia activation and for N and O insertion for molybdate vs antimonate catalysts. In addition, the isotope effect in the second H-abstraction, derived from the d_2/d_0 product mixture in 1,1-d_2-propylene ammoxidation, has been determined. When compared to the isotope effect for the rate-determining first H abstraction, the equilibrium constant for the $\pi \rightleftharpoons \sigma$ transformation and, in turn, the nature of the O- or N-inserting molybdate and antimonate species can be determined.

EXPERIMENTAL

A. Ammonia/Propylene Feed Ratio Experiments

All variable ratio NH_3/C_3H_6 experiments were performed in a continuous-flow microreactor system operating at steady state and low (<2%) conversion to approximate differential kinetic behavior. Equilibrated samples of the multicomponent molybdate (MCM) $M_a^{2+}M_b^{3+}Bi_xMo_yO_z$ (1.0 cm^3, 0.9 g) and multicomponent antimonate (MCA) $M_aM_bFe_xSb_yO_z$ (0.5 cm^3, 0.5 g) prepared by previously published methods (*3*, *5*) were placed in a 5-cm^3 stainless-steel microreactor between two layers of Pyrex wool and equilibrated in a 320°C salt bath under inert gas. A feed mixture of 1.0 C_3H_6 : 5 air : $x$$NH_3$: (1.2 − x)He (pC_3H_6 = 0.14), 1.0 C_3H_6 : 10 air : $x$$NH_3$: (1.2 − x)He (pC_3H_6 = 0.082), or 1.0 C_3H_6 : 10 air :

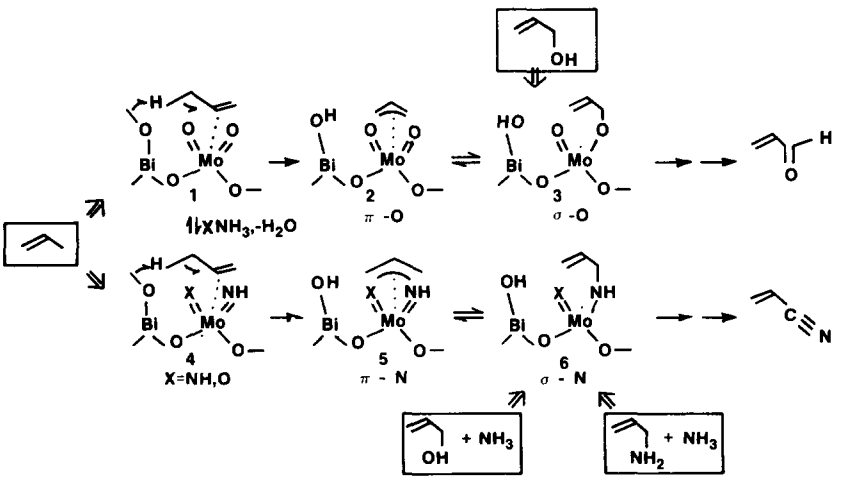

SCHEME 1. Selective oxidation and ammoxidation of propylene over molybdate catalysts.

$x NH_3 : (13.4 - x)He$ ($pC_3H_6 = 0.041$) was controlled by Brooks dual-channel mass flow controllers and fed over the catalyst at a flow rate of 29.5 cm^3/min [contact time = 1.0 sec (MCM) or 0.5 sec (MCA)] The products were collected in a 10-ml 1 or 2 *N* HCl scrubber at 0°C over a 3- to 4-hr period and analyzed by gas–liquid partition chromatography using a Varian 3700 flame ionization detector. Acrylonitrile, acetonitrile, and acrolein were analyzed on a 6 ft × $\frac{1}{8}$ in. s.s. Super Q column (Alltech) with a flow rate of 15.8 cm^3/min helium at 110°C. A temperature program of 110°C, 1 min, program rate 12°C/min, 150°C final temperature, 9 min, was used. Acrylic acid was analyzed on a 6 ft × $\frac{1}{4}$ in. glass Polyester FF column with a flow rate of 70 cm^3/min helium at 150°C isothermal operation. Gaseous products were collected by syringe and analyzed by a Carle 111 gas chromatograph using a 2 ft × $\frac{1}{8}$ in. stainless-steel column of 5% Carbowax 1000 on Chrom PAW (Supelco) and a 8 ft × $\frac{1}{8}$ in. stainless-steel column of 23% tri-*n*-butyl aconate on Chrom P (Supelco) in parallel with a 6 ft × $\frac{1}{8}$ in. stainless-steel molecular sieve 13× column, operating at 13.6 cm^3/min helium and 60°C (isothermal). All product yields were based on external standards. Yields of HCN were determined by the addition of caustic iodide followed by titration with 0.01 *M* $AgNO_3$. Ammonia breakthrough was measured by titration of the HCl scrubber with 0.125 *N* NaOH.

B. 1,1-d_2-Propylene Experiments

All isotopic experiments were performed by the pulse method using the microreactor gas chromatograph system described previously (*3*). Proton nuclear magnetic resonance (NMR) spectra were recorded on a Nicolet NT-200 (200 MHz). 1,1-d_2-Propylene (99.7 at.% 1,1-d_2, from MSD Isotopes) was combined with NH_3, air, and helium in the appropriate ratio and flushed through a 28-cm^3 loop. The loop contents were injected over $Bi_2Mo_3O_{12}$ (*3*) (2.0 cm^3, 6.7-sec contact time), USb_3O_{10} (*6*) (2.0 cm^3, 6.7-sec contact time), $M_a^{2+}M_b^{3+}Bi_xMo_yO_z$ (*3*) (0.3 cm^3, 1.0-sec contact time), and $M_aM_bFe_xSb_yO_z$ (*5*) (0.15 cm^3, 0.5-sec contact time) at 320°C, 8.9 cm^3/min helium. The catalysts were prepared by the respective references cited above. The peaks corresponding to acrylonitrile were collected in a dry ice-cooled capillary tube for NMR analysis.

RESULTS AND DISCUSSION

I. Dependence of Acrylonitrile/Acrolein Ratios on Ammonia/Propylene Feed Ratio

A. Molybdate Catalysts

1. Results. For all experiments over both MCM and MCA catalysts, conversions of propylene were 0.7–1.5%. In a representative experiment at $pC_3H_6 = 0.082$ atm, the acrylonitrile + acrolein fraction corresponded to selectivities (based on propylene) of 65–81%, with the remaining products consisting of 12–22% HCN, 6–7% acetonitrile, and 1–3% acrylic acid.

The relationship between the ammonia : propylene feed ratio and the acrylonitrile/acrolein product ratio depends on the partial pressure of reactants in the feed. At low partial pressures of feed (corresponding to $pC_3H_6 = 0.041$ atm), where the turnover of propylene is about one-third the typical high conversion reaction, the product ratio is a linear function of NH_3/C_3H_6, indicating that one ammonia molecule is involved at the N-insertion site per catalytic cycle forming acrylonitrile (Fig. 1). The single slope corresponds to the involvement of a single N-inserting species of this range studied.

At higher feed partial pressures ($pC_3H_6 = 0.082$ atm), corresponding to about two-thirds the normal turnover the product ratio is a linear function of $(NH_3)^2/C_3H_6$, corresponding to two ammonia molecules activated at the N-insertion site per acrylonitrile formed (Fig. 2). In addition, a break in the line occurs with the higher slope at low

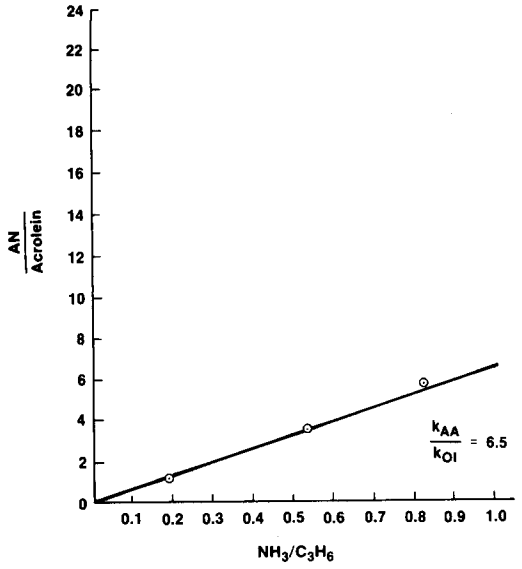

FIG. 1. Propylene ammoxidation on a multicomponent molybdate catalyst at 320°C. $p(C_3H_6)$ = 0.041 atm.

NH_3/C_3H_6 ratios, indicating that two N-inserting species are present over the range of experiments, where the first pair of ammonia molecules is activated 2.5 times faster than the second two, corresponding to the ratio of the two slopes.

At still higher feed partial pressures (pC_3H_6 = 0.14 atm) corresponding to more typical turnover rates, the exponent of the ammonia term remains 2, but only a single slope results (Fig. 2). This also corresponds to the activation of ammonia in pairs, but with the formation of only one N-inserting species over the range studied.

This situation also results if the temperature is raised under intermediate feed conditions (pC_3H_6 = 0.082 atm) (Fig. 3). Thus, the activation of ammonia becomes favored over propylene activation as the tempera-

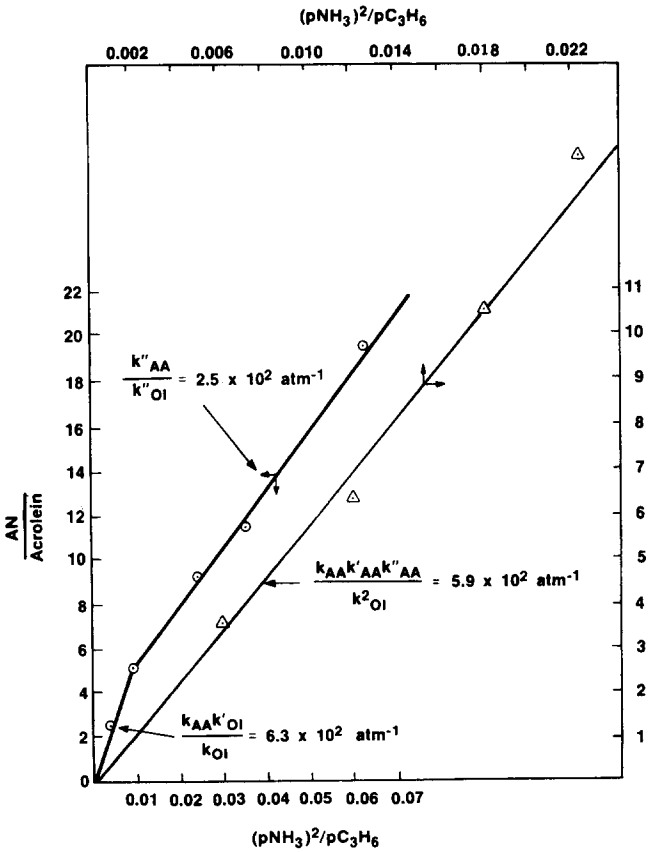

FIG. 2. Propylene ammoxidation on a multicomponent molybdate catalyst at 320°C. $p(C_3H_6)$ = 0.082 atm (⊙) and 0.14 atm (△).

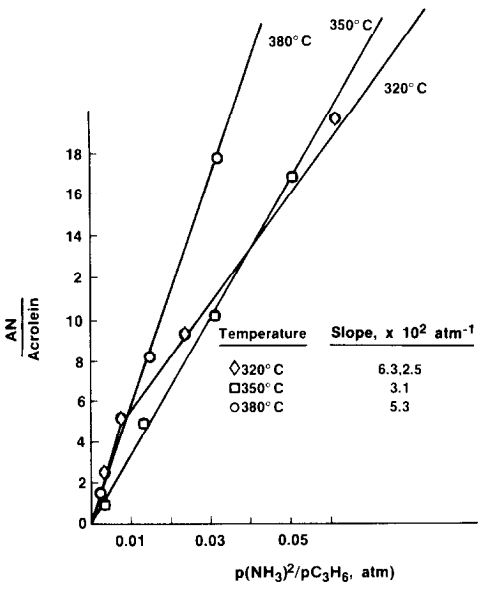

FIG. 3. Propylene oxidation/ammoxidation on a multicomponent molybdate catalyst at 320, 350, and 380°C. $p(C_3H_6) = 0.082$ atm.

ture increases due to higher activation energy for ammonia activation.

2. Kinetic model. A general kinetic scheme consistent with the results is based on the sequential activation of ammonia to form intermediate N-inserting complexes **8, 9,** and **10** (Scheme 2) in a distribution which depends on feed partial pressure and the ammonia/propylene ratio. Under the high dilution, low turnover conditions (pC_3H_6 = 0.041 atm), the major O- and N-inserting species are represented as **7** and **8,** respectively; the latter results from activation of one NH_3 molecule by **7,** giving rise to the single-slope plot with the product ratio linear with NH_3/C_3H_6.

In the intermediate turnover region (pC_3H_6 = 0.082), at low NH_3/C_3H_6 ratios (<0.24), the major O- and N-inserting species are **7** and **9,** which results from condensation of two NH_3 molecules per acryloni-

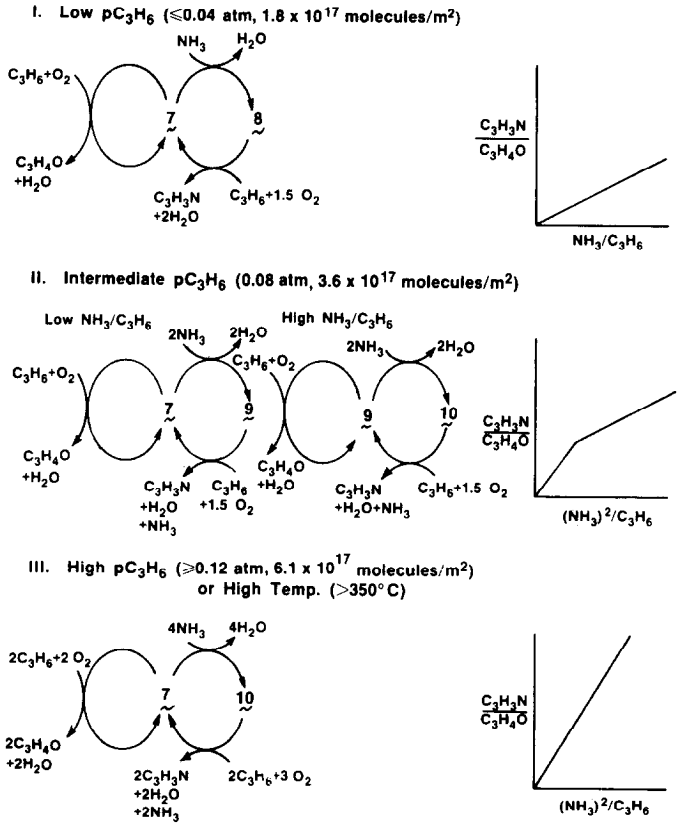

SCHEME 2. Dependence of ammonia/propylene ratio on acrylonitrile/acrolein production distribution over molybdate catalysts.

trile formed. At NH_3/C_3H_6 = 0.24, the major surface species present is **9,** which acts as both N- and O-inserting species to produce acrylonitrile and acrolein in about a 5/1 ratio. When the NH_3/C_3H_6 ratio exceeds 0.24 (high NH_3/C_3H_6, Scheme 2), enough NH_3 is now present to consecutively convert species **9** to the N-inserting species **10** by reaction with two more NH_3 molecules. Since the overall conversion of propylene does not vary greatly over the NH_3/C_3H_6 range studied, the rates of reaction of **7, 9,** and **10** with C_3H_6 are similar. Thus, species **7** activates NH_3 about 2.5 times faster than **9,** which corresponds to the ratio of the two slopes under these intermediate turnover conditions (pC_3H_6 = 0.082). This situation gives rise to the observed two-slope graph linear in $(NH_3)^2/C_3H_6$ at 320°C.

At higher feed concentration (pC_3H_6 = 0.14) or at higher temperature (350°C), where turnovers typical of stoichiometric feed (high conversion conditions) are observed, the partial pressures are high enough to convert **7** to **10** directly, and also to force two C_3H_6 molecules to react at sites **7** and **10** to form two acrolein and acrylonitrile molecules, respectively. Thus, a linear plot of the product ratio vs $(NH_3)^2/C_3H_6$ with a single slope results.

3. Active site structure and mechanism. The structure of active site **7** consistent with this kinetic scheme consists of two Mo-dioxo groups, which serve to activate ammonia sequentially to form N-inserting species **8, 9,** and **10** (Scheme 3). Species **7** and **10** exclusively insert O and N, respectively. While **8** and **9** can insert both, they insert N faster than O, as will be discussed. The reduced species corresponding to four-electron reduction (acrolein formation), symbolized by **7′**, **8′**, and **9′** reform **7, 8,** and **9,** respectively, upon reoxidation, while **7″** and **10″** result from six-electron reduction (acrylonitrile formation) and reform **7** and **10** upon reoxidation.

4. Kinetic equations. The general kinetic relationships for this mechanistic scheme

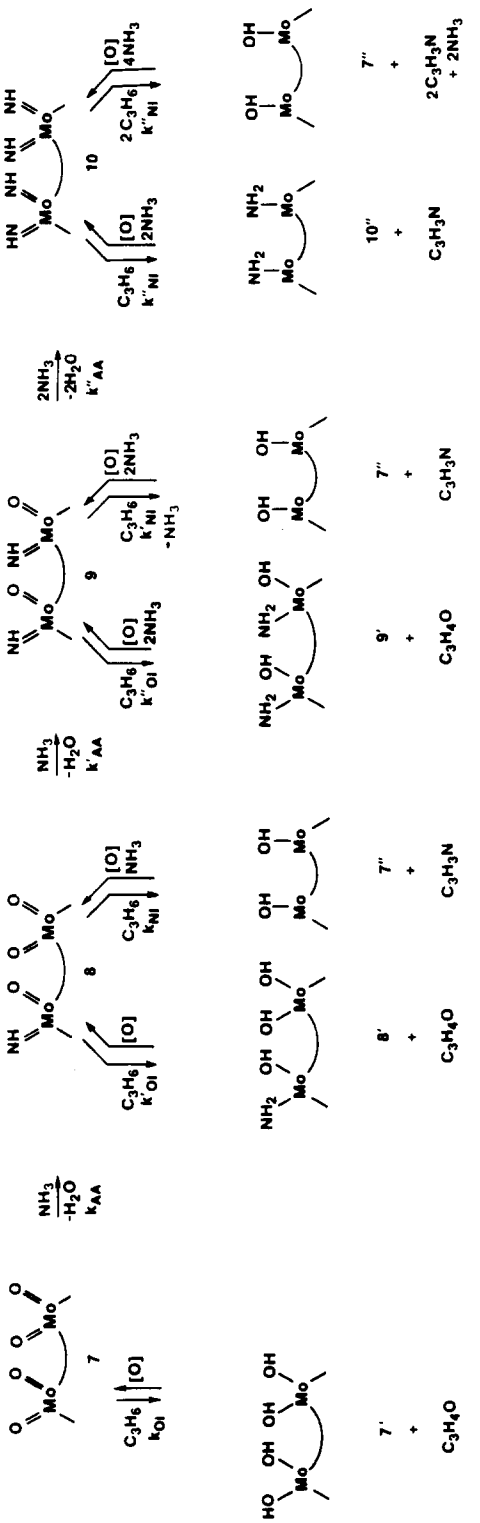

SCHEME 3. Activation of ammonia and propylene over molybdate catalysts.

(Scheme 3) may be written as follows, assuming a steady-state condition for species **8, 9,** and **10,** and that N insertion is favored over O insertion.

At low pC_3H_6 (0.041 atm), the kinetic equation is

$$\frac{r(C_3H_3N)}{r(C_3H_4O)} = \frac{k_{AA}(NH_3)}{k_{OI}(C_3H_6)} \quad (3)$$

and therefore, a plot of (C_3H_3N/C_3H_4O) vs (NH_3/C_3H_6) under differential conversion conditions should give a straight line with slope equal to k_{AA}/k_{OI} and y intercept of zero. The experimentally observed plot (Fig. 1) confirms these kinetic assumptions.

At intermediate pC_3H_6 (0.082 atm) and low NH_3/C_3H_6 (≤ 0.24), the relative rates follow the equation

$$\frac{r(C_3H_3N)}{r(C_3H_4O)} = \frac{k_{AA}k'_{OI}(NH_3)^2}{k_{OI}(C_3H_6)} \quad (4)$$

and thus a plot of (C_3H_3N/C_3H_4O) vs $(NH_3)^2/C_3H_6$ gives a straight line with slope $= k_{AA}k'_{OI}/k_{OI}$ and zero y intercept, as observed (Fig. 2).

At intermediate pC_3H_6 (0.082 atm), but high NH_3/C_3H_6 (>0.24), the equation takes the form

$$\frac{r(C_3H_3N)}{r(C_3H_4O)} = \frac{k''_{AA}(NH_3)^2}{k''_{OI}C_3H_6} + \frac{k'_{NI}}{k''_{OI}} \quad (5)$$

and thus a plot of (C_3H_3N/C_3H_4O) vs $(NH_3)^2/C_3H_6$ gives a straight line with slope k''_{AA}/k''_{OI} with a y intercept of k'_{NI}/k''_{OI}, which is the relative ratio of N/O insertion in site **9** (Scheme 3). This model is confirmed by Fig. 2, where the value of k'_{NI}/k''_{OI} is about 3. Since equal numbers of insertable N and O atoms are present in **9,** this indicates that allylic N insertion is three times faster than O insertion.

At high pC_3H_6 (0.14 atm), the equation is

$$\frac{r(C_3H_3N)}{r(C_3H_4O)} = \frac{k_{AA}k'_{AA}k''_{AA}}{k_{OI}^2}\frac{(NH_3)^2}{C_3H_6} \quad (6)$$

and therefore a plot of (C_3H_3N/C_3H_4O) vs $(NH_3)^2/C_3H_6$ will give a straight line with slope $= k_{AA}k'_{AA}k''_{AA}/k_{OI}^2$ and y intercept of zero, as observed (Fig. 2).

A complete derivation of these equations is found in the Appendix.

B. Antimonate Catalysts

1. Results. Results of experiments analogous to those for the molybdate multicomponent system were also dependent on the partial pressure reactants in the feed. At high dilution (pC_3H_6 = 0.041 atm), the product ratio was a linear function of NH_3/C_3H_6 (Fig. 4) with a zero intercept, similar to the molybdate catalyst (Fig. 1), but with an order of magnitude larger slope (k_{AA}/k_{OI} = 70).

Increasing the partial pressure of reactants ($pC_3H_6 \geq 0.082$ atm) resulted in a plot linear in $(NH_3)^2/C_3H_6$, with a zero intercept, but also about an order of magnitude larger slope (Fig. 4) than the molybdate case (Fig. 2).

2. Kinetic model. These results are consistent with a kinetic model for antimonates (Scheme 4) which is analogous to the low and high feed partial pressure cases for the molybdate system (Scheme 2). For the antimonates, however, only two N-insertion species, **12** and **13,** are involved which correspond to the activation of one and two molecules of ammonia, respectively, per active site.

3. Active site structure and mechanism. The structure of the antimonate active sites for selective oxidation (**11,** Scheme 5) is composed of bridging oxygen species which connect two Sb^{5+} and two Sb^{3+} atoms. The metal–oxygen bonding surface complex is expected to be more stable than the corresponding double-bonded species for the main group element (Sb) in contrast to a transition metal (Mo)–oxygen structure. The Sb^{3+}–O bridges serve as the H-abstracting species, while Sb^{5+}–O moieties are the active sites for NH_3 activation via formation of insertable bridging NH species (**12** and **13,** Scheme 5). The sequential activation of NH_3 in this manner explains the presence of only two regions where **12** and

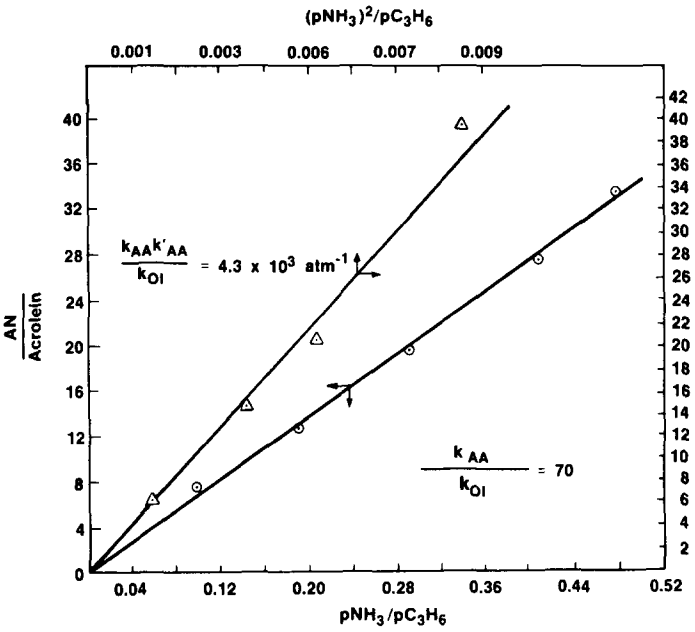

FIG. 4. Propylene ammoxidation on a multicomponent antimonate catalyst at 320°C. $p(C_3H_6)$ = 0.041 atm (⊙) and 0.082 atm (△).

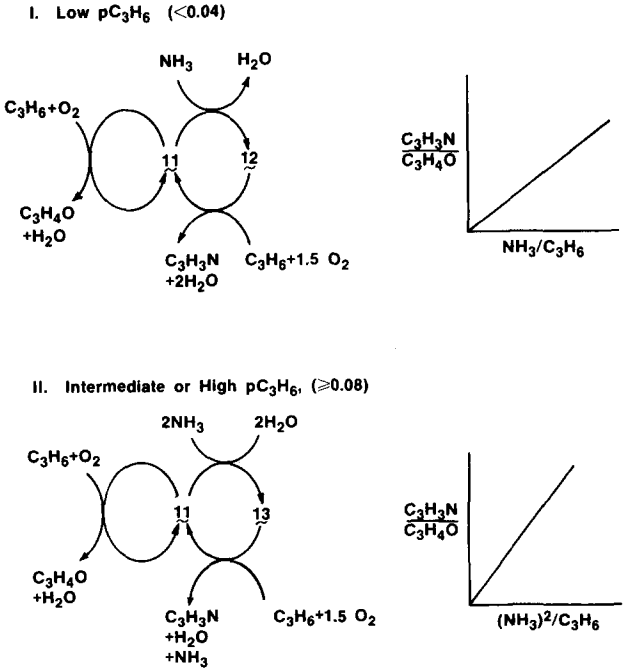

SCHEME 4. Dependence of ammonia/propylene ratio on acrylonitrile/acrolein production distribution over antimonate catalysts.

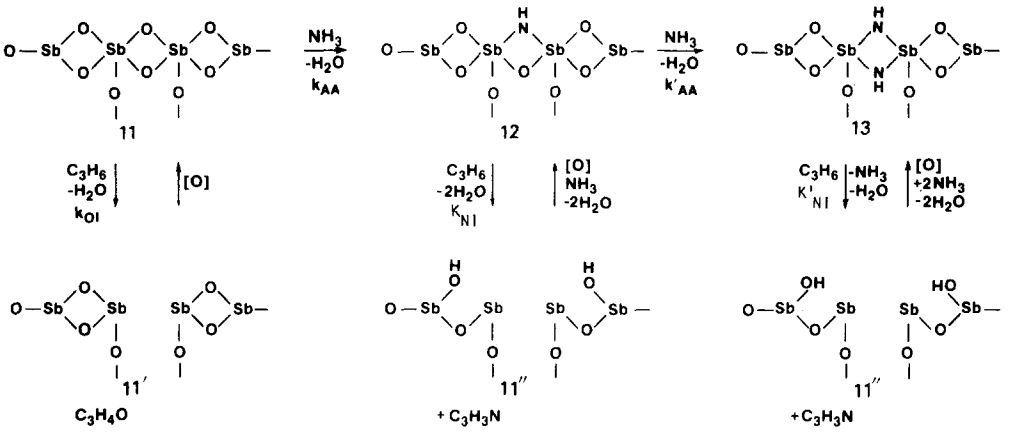

SCHEME 5. Activation of ammonia and propylene over antimonate crystals.

13 are the major acrylonitrile-forming sites at low and intermediate/high feed potential pressures, since only two O atoms (those bridging the two Sb^{5+} atoms) are capable of undergoing NH substitution.

4. Kinetic equations. By the same reasoning used for the molybdate systems, this mechanism (Scheme 5) gives rise to the following kinetic equations for low [Eq. (7)] and intermediate [Eq. (8)] feed partial pressures:

$$\frac{r(C_3H_3N)}{r(C_3H_4O)} = \frac{k_{AA}(NH_3)}{k_{OI}(C_3H_6)} \tag{7}$$

$$\frac{r(C_3H_3N)}{r(C_3H_4O)} = \frac{k_{AA}k'_{AA}}{k_{OI}}\frac{(NH_3)^2}{(C_3H_6)}. \tag{8}$$

These equations are consistent with the observed dependence of product ratio on ammonia/propylene ratio (Fig. 4).

II. 1,1-d_2-PROPYLENE REACTIONS

The proposed mechanisms for the selective oxidation and ammoxidation reactions involve oxygen- and nitrogen-inserting species which are unsaturated, double-bonded groups for molybdate catalysts (**7, 8, 9, 10,** Scheme 3), but bridging, single-bonded sites for antimonate catalysts (**11, 12, 13,** Scheme 5). Since the nature of these inserting species is very different, the reversibility of the insertion reaction (i.e., the $\pi \rightleftharpoons \sigma$ transformation) is also expected to be different. 1,1-d_2-Propylene is a sensitive probe molecule to investigate this effect (Scheme 6). The d_2/d_1-acrolein ratio expected from 1,1-d_2-propylene oxidation where $K(\pi \rightleftharpoons \sigma) = 1$ should be equal to the isotope effect k_H/k_D for the first-H abstraction (1.5–2.5 moles, typical conditions) since the σ-allyl molybdates (σ_1 and σ_2) can rapidly equilibrate. However, if K is very large, that is, the $\pi \rightarrow \sigma$ transformation is irreversible, the d_2/d_1-acrolein ratio will simply reflect the initially formed distribution of σ_1/σ_2, which is 1, since collapse of 0 (or N) on either side of the π-allyl is equally likely, and k_H and k_D are both faster than rate-determining α-H abstraction (Scheme 6). The same effect would be expected for ammoxidation to give the analogous d_2/d_0-acrylonitrile ratio, depending on the value of K.

The rate-determining nature of the first α-H abstraction for antimonates has been established by the relative rate of ammoxidation of d_0/1,1,3,3,3-d_5-propylene, from which a k_H/k_D (first H abstraction) of 2.6 can be derived. Thus, the lack of an isotope effect in the second H abstraction does not indicate that the first α-H abstraction is no longer the rate-determining step, as suggested in the literature (*8*).

Typical values for the oxidation of 1,1-d_2-propylene over molybdate ($Bi_2O_3 \cdot 2MoO_3$) and antimonate ($Sb_2O_4 \cdot 3SnO_2$) catalysts, as reported by Figueras *et al.*

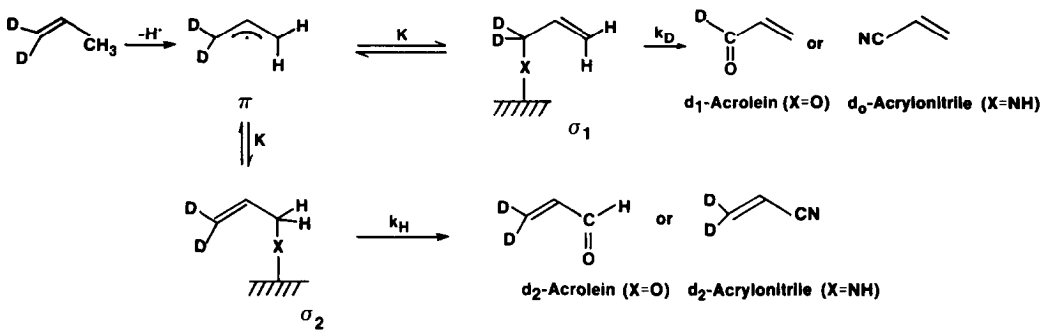

K(π⇌σ)	d_2/d_1-Acrolein	d_2/d_0 Acrylonitrile
~1.0 (reversible)	k_H/k_D (1.5-2.5)	1.5-2.5
Very large (reversible)	1.0	1.0
• Bismuth Molybdates	1.63[a] ($Bi_2O_3 \cdot 2MoO_3$)	1.59[b] ($Bi_2O_3 \cdot 3MoO_3$)
• Antimonates	0.96[a] ($Sb_2O_4 \cdot 3SnO_2$)	1.27[b] (USb_3O_{10})

SCHEME 6. Isotope effect for second hydrogen abstraction, $\pi \rightleftharpoons \sigma$, in molybdates vs antimonates. [a]Reference (*8*), 415°C. [b]This work, 320°C.

(*8*), correspond to reversible O insertion for the molybdates (d_2/d_1-acrolein = 1.63) but irreversible insertion for the antimonate catalyst (d_2/d_1-acrolein = 0.96). The corresponding d_1/d_0-acrylonitrile values comparing ammoxidation of 1,1-d_2-propylene over two molybdate- and antimonate-based systems (from this work, Table 1) indicate that the N insertion is also more reversible for ammoxidation over the molybdate systems.

Thus, the unsaturated dioxo and diimido molybdate species **7** and **10** result in reversible 0 and NH insertion, whereas the corresponding bridging antimonate sites **11** and **13** result in more irreversible 0 and NH insertion. This can be explained by the rapid formation and breaking of an allylic C–O (or C–N) bond in the π- and σ-allyl molybdates,

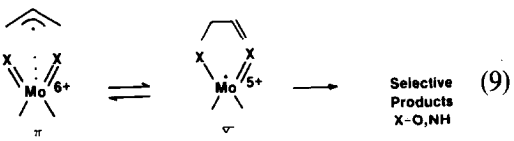

(9)

involving a single Mo center, and for which the energetics should be fairly evenly balanced. However, the formation of the σ-antimonate from this bridging π species involves the breaking of a bridging Sb–O (or N) bond:

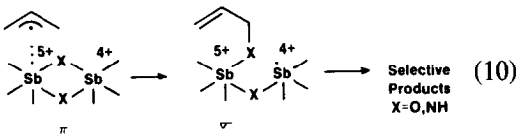

(10)

The reformation of the π species now requires that the allyl moiety in the σ form adopt a conformation in which the inserted O or N approach within bonding distance of the newly formed Sb^{4+}. Thus, entropy considerations would be expected to play a major role in the driving force for insertion in antimonates [Eq. (10)] and to contribute to the irreversible nature of the $\pi \rightarrow \sigma$ transformation when compared to the less entropy-driven molybdate system [Eq. (9)].

TABLE 1

Ammoxidation of 1,1-d_2-Propylene[a]

Catalyst	Acrylonitrile		k_H/k_D (2nd H abstraction)
	d_0	d_2	
$Bi_2Mo_3O_{12}$[b]	38.4	61.6	1.59
$M_a^{2+}M_b^{3+}Bi_xMo_yO_z$[c]	31.8	68.2	2.14
USb_3O_{10}[b]	44.0	56.0	1.27
$M_aM_bFe_xSb_yO_z$[d]	42.3	57.7	1.36

[a] 320°C reaction temperature.
[b] 6.7 sec.
[c] 1.0 sec.
[d] 0.5 sec.

Thus, once formed, the σ-antimonate is converted to selective products faster than it reverts to the π species, while the σ-molybdate reverts to the π form much faster than it undergoes the second hydrogen abstraction to form selective products. This situation appears to hold for both oxidation and ammoxidation [X = O and NH, Eqs. (9) and (10)], since antimonate catalysts give lower ratios for k_H/k_D in the second H abstraction than obtained for molybdates in both reactions (Table 1). In addition, the k_H/k_D for the second H abstraction in molybdate systems is insensitive to the NH_3/C_3H_6 ratio, indicating that the mixed oxo–imido molybdates (**8** or **9**, Scheme 3) also reversibly insert nitrogen (X = NH, O):

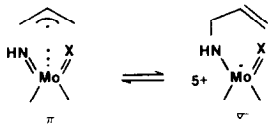

(11)

The collapse of allyl on N is, in this case, favored by about 3/1 over O insertion (Fig. 2; pC_3H_6 = 0.082; high NH_3/C_3H_6 y intercept).

A comparison of the ammoxidation of allylic-labeled propylene, allyl alcohol, and allyl amine supports the favored formation of the N vs O σ-allylic intermediate (Table 2). While both 3,3,3-d_3-propylene, and 1,1-d_2-allyl alcohol ammoxidation over single-phase molybdates result in total allylic scrambling to produce a 70:30 mixture of d_2:d_0 acrylonitrile, 1,1-d_2-allyl amine forms virtually all d_0-acrylonitrile. These results can be explained based on the favored migration of allyl from O to N

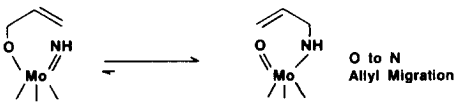

(12)

(i.e., the N σ-allyl is the more stable species), but the favored migration of H from N to O:

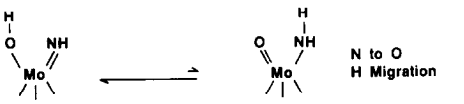

(13)

The positions of these equilibria place certain limits on the relative strength of the π component of the Mo=O and Mo=NH double bonds. In Eq. (12), a C–O bond is broken and a C–N bond is formed, which is thermodynamically uphill by about 13 kcal/mole. Thus one must gain at least that much driving force in forming Mo=O from Mo=NH. However, from Eq. (13), since an O–H bond is about 18 kcal/mole stronger than an N–H bond, the upper limit on the (Mo=O)—(Mo=NH) π-bond component is 18 kcal/mole. This range (13–18 kcal/mole) is similar to the difference between the O and N spectator atom effect as observed by Rappe and Goddard (*9*). This effect results from the fact that monooxo and monoimido Mo^{6+} species are really composed of triply bonded Mo≡O and Mo≡NH groups, where this added stabilization is 12–13 kcal/mole greater for the dioxo than for the diimido species.

Thus, this effect is an important factor in the position of these equilibria. In practical terms, the energetics of the σ-molybdates provides a system in which the oxo and imido bond energies are balanced to allow rapid formation of the imido in the presence of ammonia, but also fascile NH insertion into allyl, both of which are required of a selective ammoxidation catalyst. The application of these principles to the mechanism of ammoxidation of 1,1-d_2-allyl alcohol and 1,1-d_2-allyl amine produces allylic scrambling and retention, respectively, the ob-

TABLE 2

Ammoxidation of D-Containing Allylic Compounds over Molybdate Catalysts

Starting allylic compound	*d*- in acrylonitrile (%)	
	CD_2 = CHCN	CH_2 = CHCN
CH_2=CH—CD_3 (or CD_3=CH—CH_3)[a]	62–68	32–38
CH_2=CH—CD_2OH[b]	69	31
CH_2=CH—CD_2NH_2[c]	0	95

[a] From Table 1, this work, 430°C.
[b] Reference (*2*), MoO_3 catalyst, 430°C.
[c] Reference (*9*), $Bi_2Mo_3O_{12}$, 400°C.

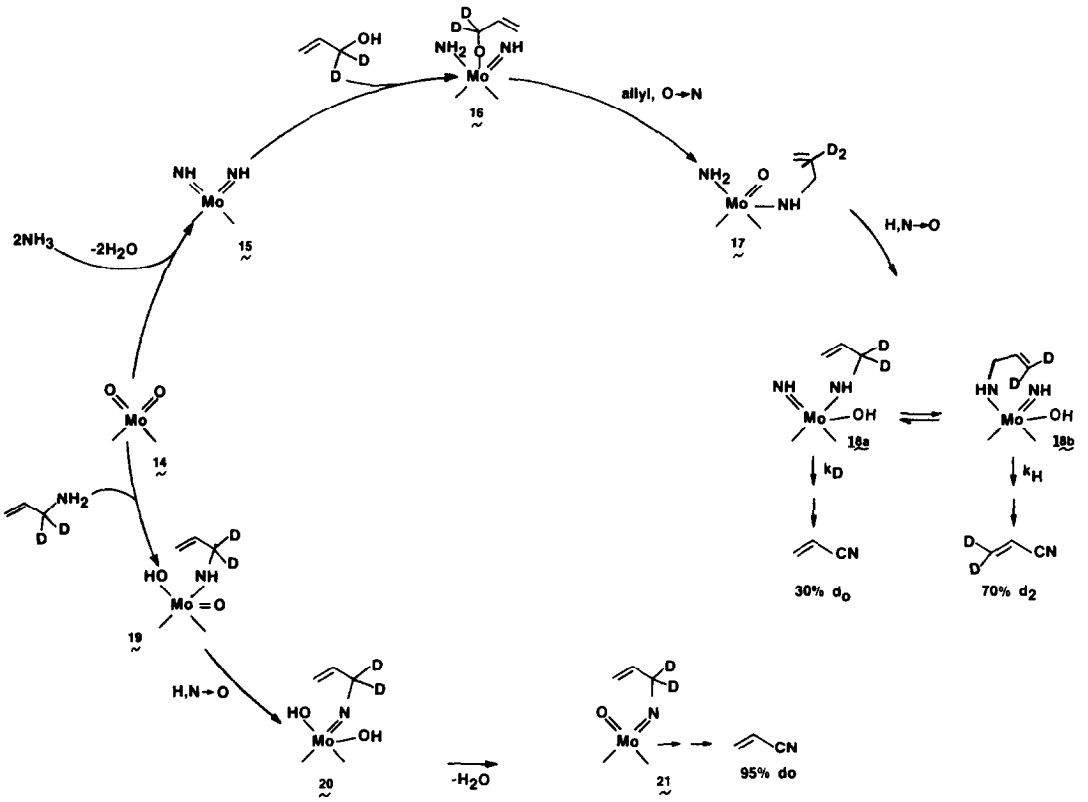

SCHEME 7. Ammoxidation of 1,1-d_2-allyl alcohol and 1,1-d_2-allyl amine.

served result (Scheme 7). In the ammoxidation of allyl alcohol, dioxo site **14** will first condense with ammonia to form diimido species **15**, with subsequent addition of 1,1-d_2-allyl alcohol across one of the Mo=NH groups to produce **16**. Migration of allyl from O to N will now occur to give **17**, which is set up to undergo rapid migration of H from N to O, producing the equilibrating structures **18a**, and **18b**, the acrylonitrile precursors. Since **18a** will form d_0-acrylonitrile at a rate (k_D) slower than will **18b** (k_H), the observed product distribution is enriched in d_2 (d_2/d_0 = 70/30).

In the ammoxidation of 1,1-d_2-allyl amine, however, allyl amine, the better nucleophile, can favorably compete with ammonia for active sites **14**, by addition across one of the Mo=O to form **19**, which will undergo rapid N to O migration of H to give **20**, and will, upon dehydration, produce **21**. The α-d atoms are now doubly allylic and are thus very labile toward abstraction. The allylic C–N bond in **21** contains more s character than in **18** (sp^2 hybridized N) and is thus stronger than that in **16**. In addition, it cannot take advantage of Mo=X resonance stabilization [Eq. (15)] which is available to **22**, (**22a** ↔ **22b**) derived from **18** [Eq. (14)].

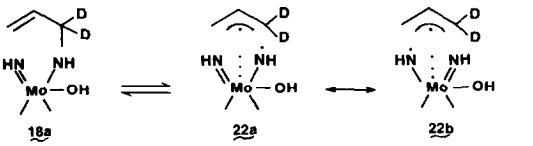

(14)

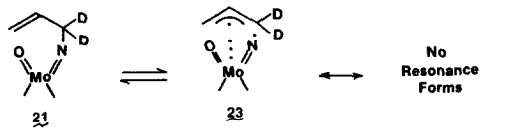

(15)

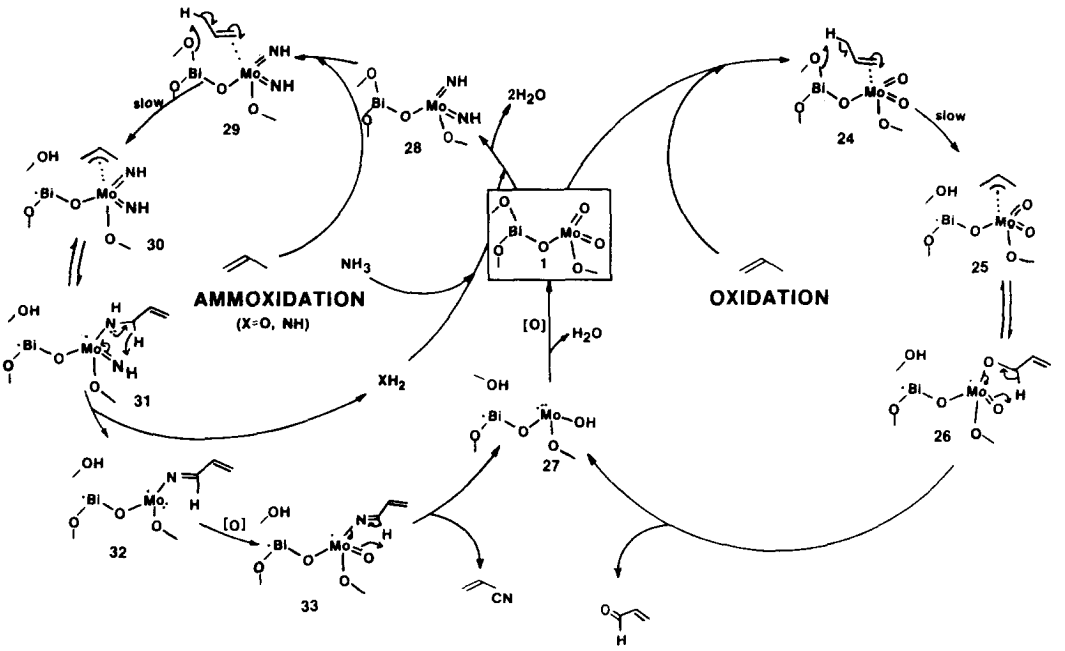

SCHEME 8. Mechanism of selective ammoxidation and oxidation of propylene over bismuth molybdates.

III. MECHANISTIC SCHEMES

A. *Molybdate Catalysts*

Under normal stoichiometric feed conditions and at high conversions, the mechanism which has been discussed previously (*4*) operates (Scheme 8). Only one Mo atom is involved which must accommodate the $4e^-$ (oxidation) and $6e^-$ (ammoxidation) reduction of the catalyst. For ammoxidation, this requires an intermediate oxidation step in which the surface species **32** must be reoxidized by bulk lattice oxygen migration. Thus, these mechanisms (Scheme 8) are characterized by a relatively deep reduction/reoxidation cycle in which bulk lattice oxygen plays a major role (*16*).

Under milder conditions (low feed partial pressures by inert gas dilution) surface sites composed of two Mo-dioxo groups operate, in which catalyst reduction can be spread out over two Mo atoms, one which serves as the O- or N-inserting element, the other as a surface redox element. For oxidation (Scheme 9), accommodation of the $4e^-$ reduction over two Mo centers results. For ammoxidation (Scheme 10), the accommodation of the $6e^-$ reduction over two Mo centers now allows a complete acrylonitrile-forming cycle without need to evoke lattice oxygen reoxidation of the surface. Thus, under these milder conditions the catalyst undergoes less deep oxidation/reduction cycles, where surface accommodation of reduction plays a major role.

The operation of two mechanistic redox regimes is supported by the work of Brazdil *et al.* (*10*). This study showed that the reoxidation of deeply reduced bismuth molybdates has an activation energy of about 25 kcal/mole (for $Bi_2Mo_3O_{12}$), corresponding to lattice oxygen diffusion, whereas a mildly reduced material had an activation energy of about 1.3 kcal/mole (for $Bi_2Mo_3O_{12}$) corresponding to surface reoxidation. Thus, under mildly reducing conditions, surface participation becomes predominant over accommodation of vacancies in the bulk which operates under

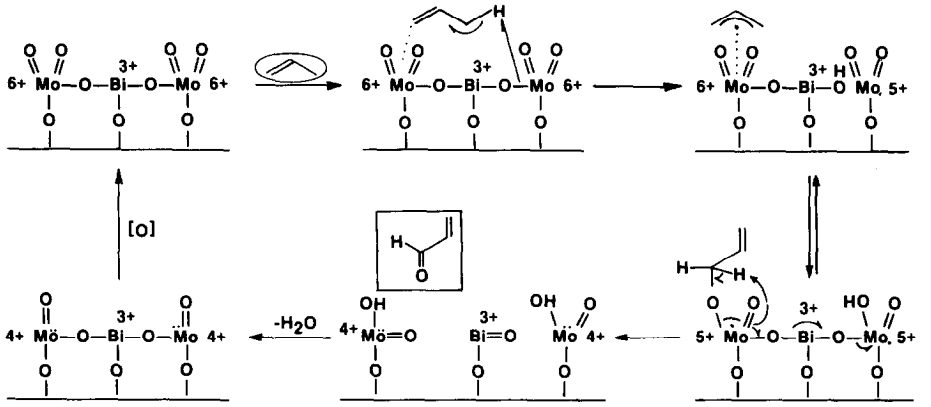

SCHEME 9. Mechanism of selective oxidation of propylene over bismuth molybdate catalysts: dilute conditions.

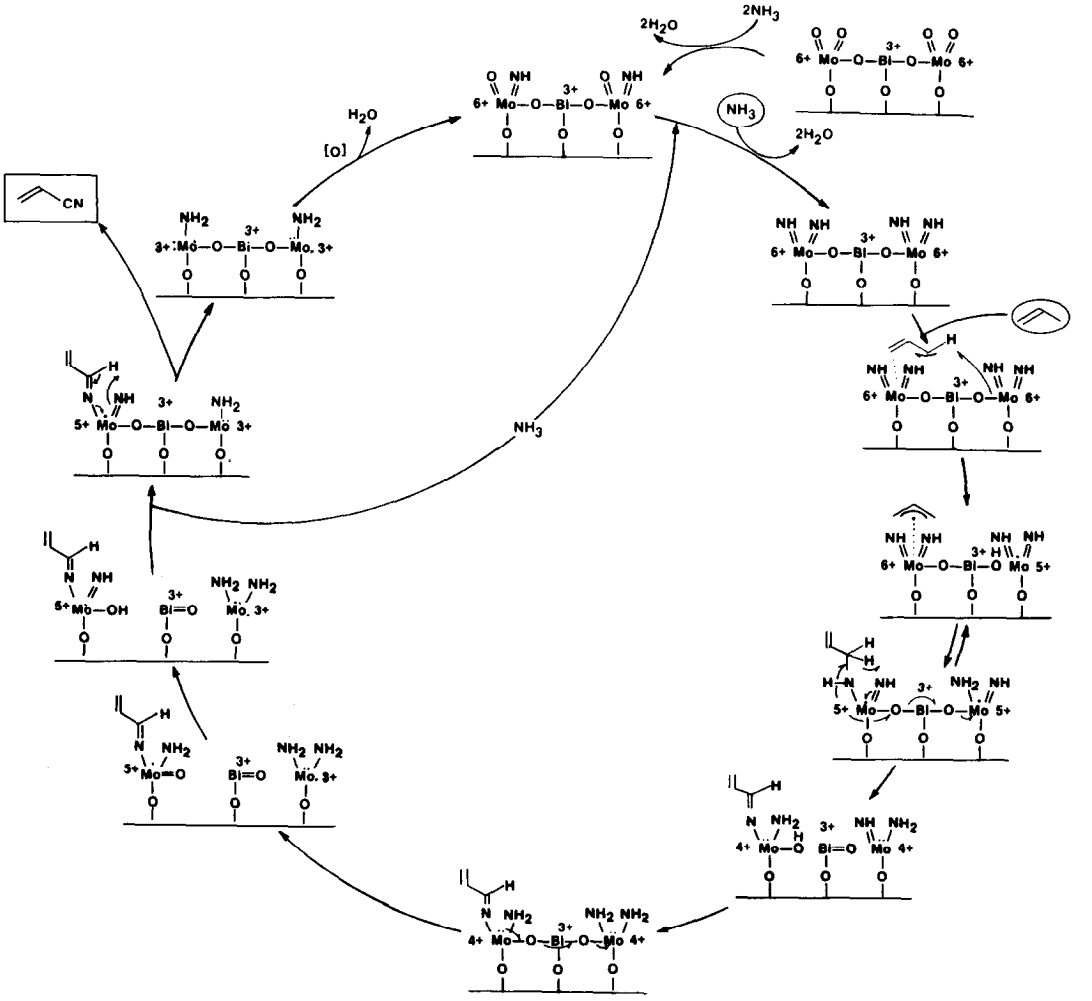

SCHEME 10. Mechanism of selective ammoxidation of propylene over bismuth molybdate catalysts: dilute conditions.

normal conditions in the Mars van Kevelin-type mechanism.

The existence of active sites containing two Mo-dioxo groups bridged by Bi–O groups is apparent from the solid-state structure of the Scheelite-derived $Bi_2Mo_3O_4$ structure containing 2 Bi and 3 Mo atoms per unit cell (Fig. 5). The boundary lines of the Scheelite unit cell are 5.6 Å, along which are located Bi atoms and vacancies in a 2 : 1 ratio in the structure. The Mo–O polyhedra, two of which have Mo-dioxo character, are stacked between these Bi "layers" and provide the structural sites for selective oxidation and ammoxidation (Schemes 9 and 10).

B. Antimonate Catalysts

The analogous mechanistic scheme for oxidation and ammoxidation over antimonates involves active sites (**34**) composed of bridging oxygen which connect two Sb^{5+} and two Sb^{3+} atoms (Scheme 11). The Sb^{5+} atoms are the chemisorption sites for propylene, the NH_3 activation sites, and the O- or N-insertion species, while bridging oxygens associated with the Sb^{3+} polyhedra perform the rate-limiting α-hydrogen abstraction. The coexistence of Sb^{3+}/Sb^{5+} pairs in active and selective antimonate catalysts has been observed by several groups, and their importance in the catalytically ac-

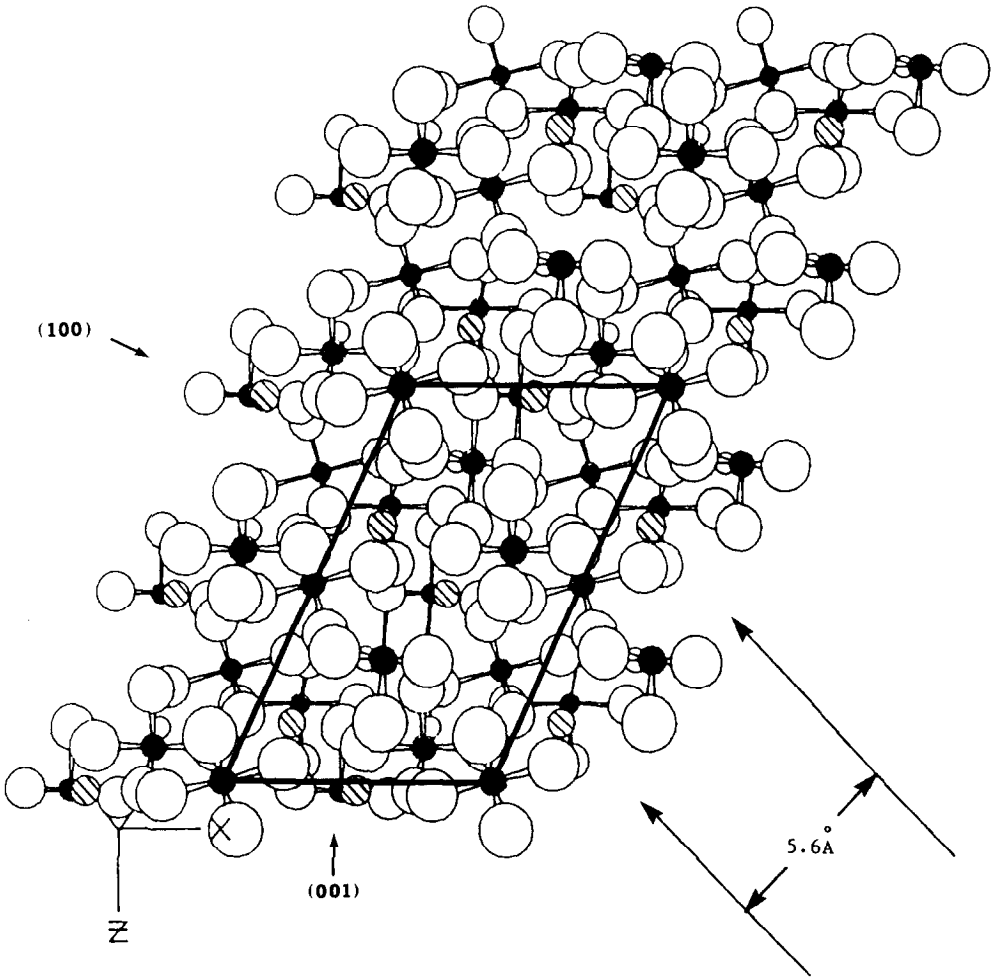

FIG. 5. Solid-state structure of α-$Bi_2Mo_3O_{12}$ (010). (⊗) Bi, (●) Mo, (○) O.

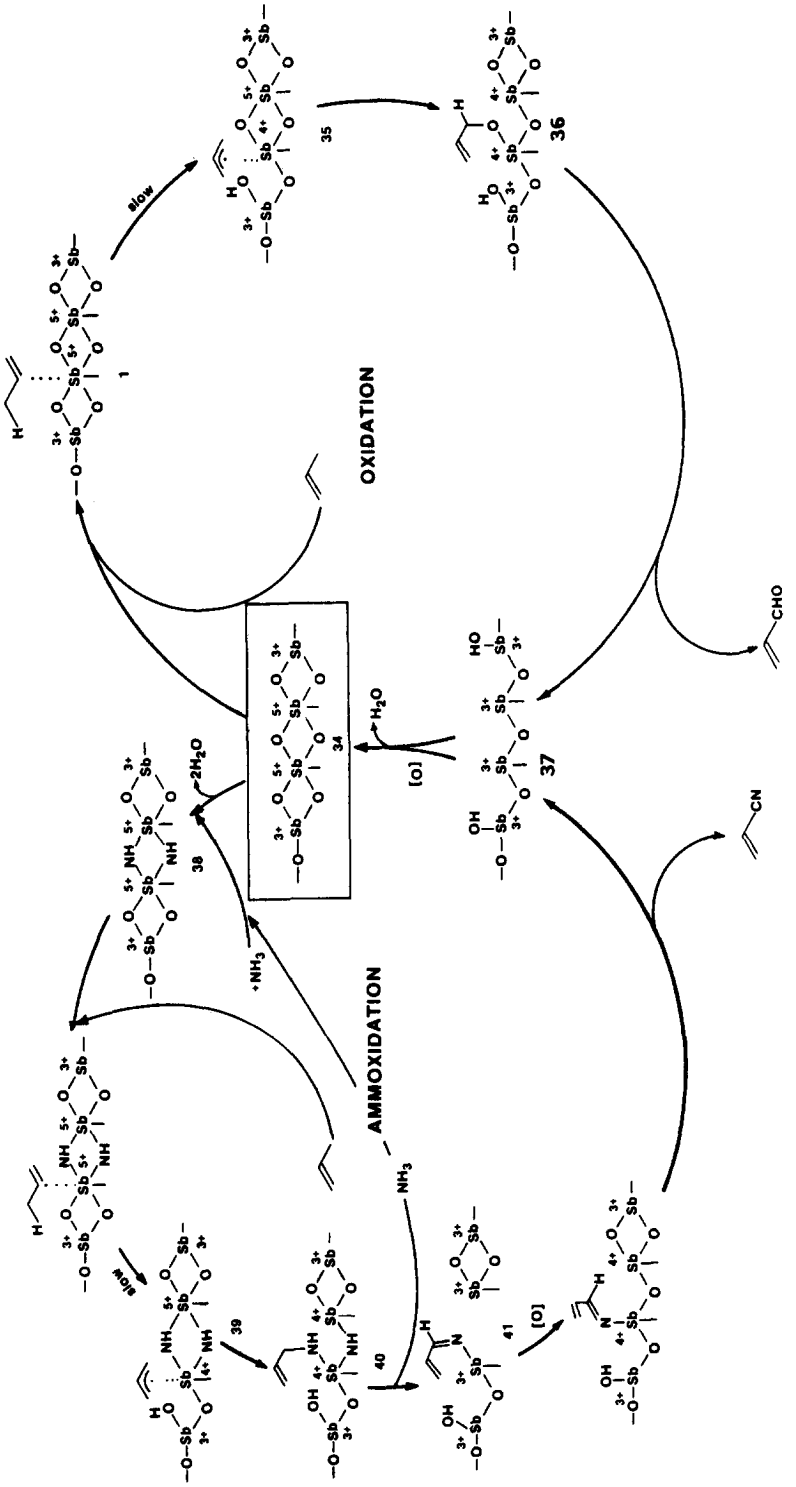

SCHEME 11. Mechanism of selective ammoxidation and oxidation of propylene over antimonates.

tive phase discussed (*11–15*). The operation of an active site (**34**, Scheme 11), which is composed of two surface Sb^{5+} atoms over the entire range of feed concentrations indicates the greater role of surface accommodation of catalyst reduction when compared to molybdate systems, as suggested in the literature (*2, 17*). This effect is reflected in the lack of an intermediate dual-slope region for antimonates (Scheme 4), as was observed for the molybdate system (Scheme 2).

In oxidation, the initially formed π-allylic species (**35**) undergoes irreversible insertion of one of the Sb^{5+} bridging oxygens to form the σ-allyl species **36**, which is converted to acrolein and reduced site **37** faster than it reverts to the π-allyl **35**. Reoxidation of **37** regenerates active site **34**. In ammoxidation, activation of ammonia occurs by formation of bridging NH species. The analogous N allyl intermediates **39** and **40** are subsequently formed which give rise to **41**, where the allyl imine moiety remains bonded to Mo. Reoxidation and subsequent H abstraction produce acrylonitrile and reduced site **37**, which is reoxidized as before.

CONCLUSIONS

The main conclusions of this work are:

1. For molybdate catalysts, two Mo-dioxo groups are present at the catalytic sites which activate NH_3 pairwise by successive formation of Mo-diimido groups.

2. Under low turnover (dilute feed, low temperature, 320°C) conditions, both Mo sites can participate in the catalytic cycle, one as the O- or N-inserting species, the other as a redox element, and surface accommodation of catalyst reduction is important.

3. At higher turnovers (higher concentrations of feeds or higher temperatures, $\geq$ 350°C) selective products result from reaction of propylene at one Mo-dioxo or -diimido site, and bulk lattice participation is the major mechanism for accommodation of catalyst reduction.

4. Favored O to N allyl migration but N to O hydrogen migration indicates that the π component of the Mo=O multiple bond is ~15 kcal/mole stronger than that for the Mo=N multiple bond in the surface monooxo and monoimido allylic intermediates, respectively.

5. Active sites of antimonate catalysts are composed of H-abstracting Sb^{3+}–O groups and O-inserting or NH_3-activating/N-inserting Sb^{5+}–O bridging oxygens.

6. The ammonia/propylene activation ratio (first-order kinetics) for antimonates is about 10 times that of molybdate catalysts.

7. Conversion of π-allyl to σ-antimonate is less reversible than the corresponding σ-molybdate formation, which represents insertion into bridging vs unsaturated metal–O (or –N) bonds, respectively.

8. For antimonates, surface participation accounts for a major portion of catalyst reduction under normal reaction conditions (high turnover), as opposed to the bulk participation (Mars Van-Krevelen) mechanism which operates for molybdates.

APPENDIX

The general kinetic relationships (Section I.A.4) were derived for each feed dilution condition as follows, using species shown in Scheme 3:

1. Low $p_{C_3H_6}$ (0.041 atm)

$$\frac{r(C_3H_3N)}{r(C_3H_4O)} = \frac{k'_{NI}(\mathbf{8})(C_3H_6)}{k_{OI}(\mathbf{7})(C_3H_6) + k'_{OI}(\mathbf{8})(C_3H_6)}. \quad (16)$$

Assuming a steady-state condition for **8**,

$$k_{NI}(\mathbf{8})(C_3H_6) + k'_{OI}(\mathbf{8})(C_3H_6) = k_{AA}(\mathbf{7})(NH_3), \quad (17)$$

which, since N insertion is favored over O insertion (*4*), i.e., $k_{NI} \gg k'_{PA}$, reduces to

$$k_{NI}(\mathbf{8})(C_3H_6) = k_{AA}(\mathbf{7})(NH_3). \quad (18)$$

Assuming k_{OI} (**7**) $\gg k'_{OI}$ (**8**) over this region, Eq. (16) reduces to

$$\frac{r(C_3H_3N)}{r(C_3H_4O)} = \frac{k_{NI}(\mathbf{8})(C_3H_6)}{k_{PA}(\mathbf{7})(C_3H_6)}.$$

Combining with Eq. (18) this reduces to

$$\frac{r(C_3H_3N)}{r(C_3H_4O)} = \frac{k_{AA}(NH_3)}{k_{PA}(C_3H_6)}.$$

2. INTERMEDIATE pC_3H_6 (0.081 atm)

(a) Low NH_3/C_3H_6 (< 0.24)

$$\frac{r(C_3H_3N)}{r(C_3H_4O)} = \frac{k'_{NI}(\mathbf{9})(C_3H_6)}{k_{PA}(\mathbf{7})(C_3H_6) + k''_{PA}(\mathbf{9})(C_3H_6)}. \quad (19)$$

At steady-state conditions for **9**,

$$k'_{NI}(\mathbf{9})(C_3H_6) + k''_{OI}(\mathbf{9})(C_3H_6) = k_{AA}k'_{AA}(NH_3)^2(\mathbf{7}) \quad (20)$$

and assuming that N insertion is again favored over O insertion, $k'_{NI} \gg k''_{OI}$, and that $k_{OI}(\mathbf{7}) \gg k'_{OI}(\mathbf{9})$ over this region, Eq. (19) reduces to

$$\frac{r(C_3H_3N)}{r(C_3H_4O)} = \frac{k_{AA}k'_{AA}(NH_3)^2}{k_{OI}(C_3H_6)}. \quad (4)$$

(b) High NH_3/C_3H_6 ($\geq$ 0.24)

$$\frac{r(C_3H_3N)}{r(C_3H_4O)} = \frac{k''_{NI}(\mathbf{10})(C_3H_6) + k'_{NI}(\mathbf{9})(C_3H_6)}{k''_{OI}(\mathbf{9})(C_3H_6)} = \frac{k''_{NI}(\mathbf{10})(C_3H_6)}{k''_{OI}(\mathbf{9})(C_3H_6)} + \frac{k'_{NI}}{k''_{OI}}. \quad (21)$$

At steady state for **10**,

$$k''_{NI}(\mathbf{10})(C_3H_6) = k''_{AA}(\mathbf{9})(NH_3)^2 \quad (22)$$

and thus,

$$\frac{r(C_3H_3N)}{r(C_3H_4O)} = \frac{k''_{AA}(NH_3)^2}{k''_{OI}(C_3H_6)} + \frac{k'_{NI}}{k''_{OI}}. \quad (5)$$

3. HIGH pC_3H_6 (0.14 atm)

$$\frac{r(C_3H_3N)}{r(C_3H_4O)} = \frac{k^2_{NI}(\mathbf{10})^{1/2}(C_3H_6)}{k^2_{OI}(\mathbf{7})^{1/2}(C_3H_6)}. \quad (23)$$

At steady state for **10**,

$$k^2_{NI}(\mathbf{10})^{1/2}(C_3H_6) = k_{AA}k'_{AA}k''_{AA}(NH_3)^2(\mathbf{7})^{1/2}, \quad (24)$$

and thus,

$$\frac{r(C_3H_3N)}{r(C_3H_4O)} = \frac{k_{AA}k'_{AA}k''_{AA}(NH_3)^2}{k^2_{OI}(C_3H_6)}. \quad (6)$$

ACKNOWLEDGMENTS

The authors wish to thank Dr. Ken Gallaher and Mr. Terry Hammond of the Surface and Molecular Spectroscopy Group at Sohio Research, and Dr. Raymond G. Teller for computer graphics.

REFERENCES

1. Grasselli, R. K., Burrington, J. D., and Brazdil, J. F., *Faraday Soc. Discuss.* **72,** 204 (1982); Grasselli, R. K., and Burrington, J. D., *Adv. Catal.* **30,** 133 (1981), and references therein.
2. Trifiro, F., Lambri, C., and Pasqurn, I., *Chem. Ind. (Milan)* **53,** 339 (1971).
3. Burrington, J. D., Kartisek, C. T., and Grasselli, R. K., *J. Catal.* **63,** 235 (1980).
4. Burrington, J. D., Kartisek, C. T., and Grasselli, R. K., *J. Catal.* **81,** 489 (1983).
5. Callahan, J. L., Grasselli, R. K., and W. R. Knipple, U.S. Patent 3,546,138 (Dec. 8, 1970); Yoshino, T., Saito, S., Sasaki, Y., and Nakamura, Y., U.S. Patent 3,657,155 (Apr. 13, 1972).
6. Grasselli, R. K., and Suresh, D. D., *J. Catal.* **25,** 273 (1972).
7. Goddard, W. A., III, private communication.
8. Portefaix, J. J., Figueras, F., and Forrissier, M., *J. Catal.* **63,** 307 (1980).
9. Rappe, A. K., and Goddard, W. A., III, *J. Amer. Chem. Soc.* **104,** 448 (1982).
10. Brazdil, J. F., Suresh, D. D., and Grasselli, R. K., *J. Catal.* **66,** 347 (1980).
11. Berry, F. J., *J. Catal.* **73,** 349 (1982).
12. Yamazoe, N., Aso, I., Amamoto, T., and Seiyama, T., *in* "Proceedings, 7th International Congress on Catalysis 1980," Part B, p. 1239 (1981).
13. Aso, I., Furukawa, S., Yamazoe, N., and Seiyama, T., *J. Catal.* **64,** 29 (1980).
14. Figueras, F., *et al., J. Chem. Soc. Faraday Trans. 1* **76,** 1652 (1980).
15. Pyke, D. R., Reid, R., and Tiley, R. J. D., *J. Chem. Soc. Faraday Trans. 1* **76,** 1174 (1980).
16. Keulks, G. W., Krenzke, L. D., and Notermann, T. M., *Adv. Catal.* **27,** 183 (1978).
17. Delobel, R., Baussart, H., Levoy, J. M., Grimblot, J., and Gengembre, L., *J. Chem. Soc. Faraday Trans. 1* **79,** 879 (1983).